Crystal-field states of Kondo lattice heavy fermions CeRuSn₃ and CeRhSn₃

V. K. Anand,[1,2,*] D. T. Adroja,[1,3,†] D. Britz,[3] A. M. Strydom,[3,4] J. W. Taylor,[1] and W. Kockelmann[1]

[1]*ISIS Facility, Rutherford Appleton Laboratory, Chilton, Didcot, Oxon, OX11 0QX, United Kingdom*

[2]*Helmholtz-Zentrum Berlin für Materialien und Energie GmbH, Hahn-Meitner Platz 1, D-14109 Berlin, Germany*

[3]*Highly Correlated Matter Research Group, Physics Department, University of Johannesburg, P.O. Box 524,
Auckland Park 2006, South Africa*

[4]*Max Planck Institute for Chemical Physics of Solids, Nöthnitzerstr. 40, 01187 Dresden, Germany*

Inelastic neutron scattering experiments have been carried out to determine the crystal-field states of the Kondo lattice heavy fermions CeRuSn₃ and CeRhSn₃. Both the compounds crystallize in LaRuSn₃-type cubic structure (space group $Pm\bar{3}n$) in which the Ce atoms occupy two distinct crystallographic sites with cubic ($m\bar{3}$) and tetragonal ($\bar{4}m.2$) point symmetries. The INS data of CeRuSn₃ reveal the presence of a broad excitation centered around 6–8 meV, which is accounted by a model based on crystal electric field (CEF) excitations. On the other hand, the INS data of isostructural CeRhSn₃ reveal three CEF excitations around 7.0, 12.2, and 37.2 meV. The neutron intensity sum rule indicates that the Ce ions at both cubic and tetragonal Ce sites are in Ce³⁺ state in both CeRuSn₃ and CeRhSn₃. The CEF level schemes for both the compounds are deduced. We estimate the Kondo temperature $T_{\rm K} = 3.1(2)$ K for CeRuSn₃ from neutron quasielastic linewidth in excellent agreement with that determined from the scaling of magnetoresistance which gives $T_{\rm K} = 3.2(1)$ K. For CeRhSn₃, the neutron quasielastic linewidth gives $T_{\rm K} \approx 4.6$ K. For both CeRuSn₃ and CeRhSn₃, the ground state of Ce³⁺ turns out to be a quartet for the cubic site and a doublet for the tetragonal site.

I. INTRODUCTION

Ce-based heavy fermion systems, whose electronic ground-state properties are determined by strongly competing Ruderman-Kittel-Kasuya-Yosida (RKKY) and Kondo interactions, present very interesting physics [1–6]. While RKKY interaction tends to establish a long-range order, Kondo interaction causes screening of $4f$ moments (below a characteristic Kondo temperature $T_{\rm K}$) leading to a paramagnetic ground state and a quantum critical behavior is realized when the strength of these interactions become comparable, i.e., at the boundary between the magnetically ordered and paramagnetic states. A wide range of intriguing physical properties is seen in the proximity of a quantum critical point (QCP) [1–6]. One can achieve QCP by tuning the electronic ground state of antiferromagnetically ordered systems using an external pressure, magnetic field, or chemical doping and because of this Ce compounds are ideal for the study of the physics of quantum critical phenomena. For example, a pressure-induced superconductivity is observed in the antiferromagnet CeCoGe₃ at a critical pressure of 5.5 GPa and a partial substitution of Ge by Si leads to a non-Fermi liquid behavior and quantum criticality in CeCo(Ge$_{1-x}$Si$_x$)₃ [7–12].

In this paper, we focus on two Kondo lattice heavy fermions CeRuSn₃ and CeRhSn₃, both of which form in a cubic structure (space group $Pm\bar{3}n$, No. 223) with LaRuSn₃ structure as the prototype structure [13]. This LaRuSn₃-type cubic structure consists of two distinct cages formed by the three-dimensional network of trigonal RuSn₆ prisms which are occupied by Ce atoms, thus there are two distinct Ce-sites. Earlier investigations of physical properties of CeRuSn₃ by

Fukuhara *et al.* [14] and Takayanagi *et al.* [15] revealed a large electronic coefficient γ in heat capacity $C_{\rm p}(T)$ and a logarithmic increase ($-\ln T$ behavior) in electrical resistivity $\rho(T)$, thus characterizing CeRuSn₃ as a Kondo lattice heavy fermion system. They noticed an absence of coherence effect in resistivity as well as Hall effect, accordingly they suggested the possibility of existence of atomic disorder in CeRuSn₃ [14,15]. They also found a sharp anomaly at 0.5 K in ac susceptibility with an accompanying broad peak in $C_{\rm p}/T$ versus T which they correlated to a magnetic phase transition with an open possibility of antiferromagnetic ordering or spin-glass transition [15]. Fukuhara *et al.* [16] investigated the effect of Sn content on the physical properties of CeRuSn$_x$ ($2.85 \leqslant x \leqslant 3.15$) and found that the Sn deficiency influences the physical properties. Three phase transitions at 33, 4, and 1.3 K were suggested in CeRuSn₂.₉₁ with an antiferromagnetic ground state below 1.3 K [16,17]. In contrast, no observable change was noticed in the electronic states with Sn content of CeRuSn$_x$ for $x = 2.85$, 3.0, and 3.15 in core-level photoemission spectroscopy [18].

In our effort to understand the nature of the magnetic transition in CeRuSn₃, we have investigated this compound using various techniques. Our preliminary results are reported in Ref. [19]. Our $C_{\rm p}(T)$ data confirmed the heavy fermion behavior with $\gamma \geqslant 212(2)$ mJ/mol K² and $\rho(T)$ data confirmed the Kondo lattice feature in CeRuSn₃ [19]. We found a broad peak in $C_{\rm p}/T$ versus T near 0.6 K and an anomaly in dc $\chi(T)$ near 0.6 K. Further, we noticed an irreversibility between the zero-field-cooled and field-cooled $\chi(T)$ data [19], which is not consistent with the antiferromagnetic model. Furthermore, no long-range antiferromagnetic order was inferred from the muon spin relaxation (μSR) measurement. However, the μSR data are consistent with glassy spin dynamics [19]. Thus our investigations rule out the possibility of previously suggested antiferromagnetic transition in CeRuSn₃.

*vivekkranand@gmail.com

†devashibhai.adroja@stfc.ac.uk

014440-1

Our investigations of physical properties of $CeRhSn_3$ have revealed a complex magnetic ground state and moderate heavy fermion behavior in this compound [20]. The T dependence of ρ revealed the Kondo lattice behavior. Both dc $\chi(T)$ and $C_p(T)$ exhibit two well pronounced anomalies near 4 K and 1 K, while the former seems to be related to a transition to ferrimagnetic ordering, the latter seems to be related to a transition from the ferri- to a ferro-magnetic order below 1 K [20]. Interestingly, the ac $\chi(T)$ of $CeRhSn_3$ presents an unexplained frequency dependence where the temperature of the 4 K anomaly is found to decrease with increasing frequency. A long-range ordered state below 1 K was inferred from the μSR study on $CeRhSn_3$, however, no such transition was detected at 4 K in the μSR and powder neutron diffraction studies [20]. The isostructural $PrRhSn_3$ was found to exhibit a ferromagnetic cluster spin-glass behavior [21] in which a frustrated magnetic ground state is believed to result from the dynamic fluctuations of the crystal-field levels similar to the case of spin-glass systems $PrAu_2Si_2$ [22] and $PrRuSi_3$ [23].

Here we extend our investigations on $CeRuSn_3$ and $CeRhSn_3$ and report the results of inelastic neutron scattering (INS) measurements on these compounds. The INS data are analyzed using a model based on CEF providing information about the crystal-field states of Ce in these compounds. A comparative study of physical properties and INS results of the two compounds is presented.

II. EXPERIMENTAL

The polycrystalline samples of $CeRuSn_3$ and $CeRhSn_3$ as well as their nonmagnetic analogs $LaRuSn_3$ and $LaRhSn_3$ were prepared by the standard arc melting technique using high purity elements in stoichiometric ratios and subsequent annealing at 900 °C for 7 days as detailed in Refs. [20,21]. The crystal structures and the qualities of the samples were checked by powder x-ray diffraction (XRD) using Cu K_α radiation, which confirmed the single phase nature and $LaRuSn_3$-type cubic crystal structure of all four. Chemical composition was checked by energy dispersive x-ray (EDX) analysis using a scanning electron microscope (SEM), which revealed the desired 1:1:3 stoichiometry. The specific heat was measured by the relaxation method using a physical properties measurement system (PPMS, Quantum Design). Electrical resistivity was measured by the standard four probe method using PPMS.

The room temperature neutron diffraction (ND) experiment was performed on the powdered sample of $CeRuSn_3$ using the ROTAX diffractometer at the ISIS facility of Rutherford Appleton Laboratory, Didcot, U.K. The inelastic neutron scattering experiment on $CeRuSn_3$ was performed with the HET time of flight (TOF) spectrometer at ISIS. The INS experiments on $CeRhSn_3$ and $LaRhSn_3$ were performed on the MARI TOF spectrometer. The powdered samples of these materials were wrapped in thin Al foils and mounted inside thin-walled cylindrical Al cans. Low temperatures down to 4.5 K were obtained by cooling the sample mounts in a top-loading closed cycle refrigerator with He-exchange gas. The INS data were collected for scattering angles between 3° and 135° using neutrons with incident energies $E_i = 11, 23,$ and 50 meV for $CeRuSn_3$ on HET and $E_i = 23$ and 50 meV for $CeRhSn_3$ and $LaRhSn_3$ on MARI.
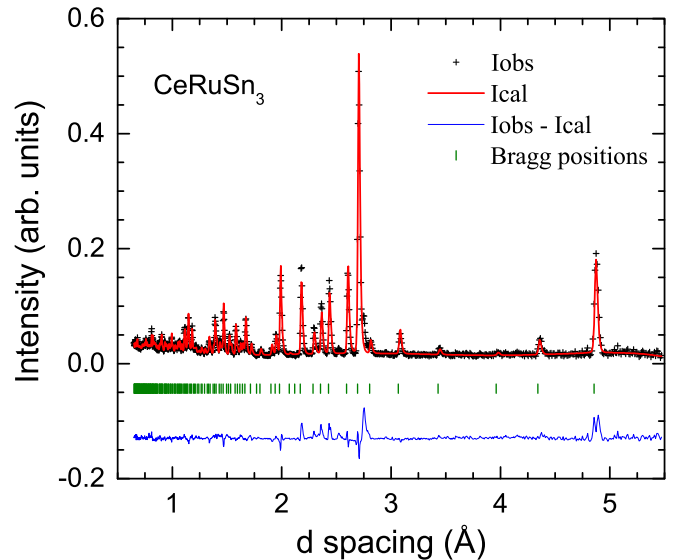

FIG. 1. Powder neutron diffraction pattern of $CeRuSn_3$ recorded at room temperature. The solid line through the experimental points is the Rietveld refinement profile calculated for $LaRuSn_3$-type cubic (space group $Pm\bar{3}n$) structure. The short vertical bars mark the fitted Bragg peak positions. The lowermost curve represents the difference between the experimental and calculated intensities.

III. CRYSTALLOGRAPHY

A. Powder neutron diffraction study on CeRuSn₃

The room temperature powder neutron diffraction pattern of $CeRuSn_3$ is shown in Fig. 1. The ND data were refined by using the program GSAS [24]; the structural refinement profile is shown in Fig. 1. The refinement confirmed the $LaRuSn_3$-type cubic structure (space group $Pm\bar{3}n$) of $CeRuSn_3$ and revealed the single-phase nature of the sample. While refining the ND data we checked for the possibility of site mixing of Ru and Sn, however the difference in the scattering lengths of Ru and Sn is too small to produce a noticeable change in the observed intensity for weak site disorder of a few percent. Thus the ND data are of not much help in resolving the possibility of weak atomic disorder suggested in Refs. [14,15]. The refined crystallographic parameters obtained from the least squares refinement of neutron diffraction data are listed in Table I. The structure parameters obtained from the refinements of neutron diffraction and x-ray diffraction data are similar and agree well with the literature values [13,14]. The crystallographic data for $CeRhSn_3$ can be found in Ref. [20].

B. Crystal structure

The $LaRuSn_3$-type cubic structure of $CeRuSn_3$ and $CeRhSn_3$ is illustrated in Fig. 2. The Ru atoms occupying 8e sites have trigonal prismatic coordination and sit within the tilted $RuSn_6$ prisms formed by six Sn atoms. These tilted $RuSn_6$ prisms form a three dimensional network and one can observe two different cages, which are occupied by Ce atoms. Thus the structure allows two distinct sites for Ce atoms with different near-neighbor environment and coordination numbers (CN). The Ce atoms sitting at 2a sites referred as Ce1 have a CN of 20 whereas the Ce atoms sitting at 6d sites referred as Ce2 have CN of 16 [13,25]. Ce1 has a near-neighbor

TABLE I. Crystallographic parameters obtained from the Rietveld refinement of room temperature powder neutron diffraction data of CeRuSn$_3$ using the program GSAS. Profile reliability factor $R_p = 10.54\%$ and weighted profile R-factor $R_{wp} = 9.04\%$.

Structure			LaRuSn$_3$-type cubic		
Space group			$Pm\bar{3}n$, No. 223		
Formula units/unit cell			8		
Lattice parameters					
a (Å)			9.7340(4)		
V_{cell} (Å^3)			922.3(1)		
Atomic coordinates					
Atom	Wyckoff symbol	x	y	z	U_{iso} (Å^2)
Ce1	2a	0	0	0	0.072(6)
Ce2	6d	1/4	1/2	0	0.0062(8)
Ru	8e	1/4	1/4	1/4	0.0075(5)
Sn	24k	0	0.3117(2)	0.1571(2)	0.0202(7)

environment of same chemical species consisting of 12 Sn atoms. On the other hand, Ce2 has both Ru and Sn as neighbors. The two Ce sites have different point symmetries—while Ce1 has a cubic point symmetry ($m\bar{3}$), Ce2 has a tetragonal point symmetry ($\bar{4}m.2$).

IV. CeRuSn$_3$

A. Inelastic neutron scattering study

Figure 3 shows the INS scattering response, plotted as color-coded intensity maps, at low-Q from CeRuSn$_3$ measured with $E_i = 11, 23$, and 50 meV on HET at 4.5 K. There is a clear evidence of magnetic excitations centered around 6–8 meV in the 23 and 50 meV data. On the other hand, 11-meV data reveal the presence of strong quasielastic scattering centered on zero-energy transfer. The phonon reference compound LaRhSn$_3$ did not reveal any strong phonon scattering at low-Q at 4.5 K. This indicates that the excitations seen at low-Q in CeRuSn$_3$ are due to crystal-field excitations of the Ce ions. It is to be noted that there are two crystallographic sites for Ce atoms in CeRuSn$_3$. One Ce site (called Ce1) has cubic

point symmetry, $m\bar{3}$, while another Ce site (called Ce2) has tetragonal point symmetry, $\bar{4}m.2$ (Fig. 2). When subject to CEF the sixfold degenerate cubic point symmetry $J = 5/2$ state of Ce^{3+} ion will split into a doublet (twofold degenerate, Γ_7) and a quartet (fourfold degenerate, Γ_8). Hence for the cubic Ce site, we expect one CEF excitation at all temperatures. On the other hand, under the action of CEF, the tetragonal point symmetry $J = 5/2$ state of Ce^{3+} ion will split into three doublets. Thus, if there is no accidental degeneracy, we normally expect two CEF excitations from the ground state of the tetragonal site Ce. However, if the ground state is pure $J_z = \pm 1/2$ and excited states are pure $J_z = \pm 3/2$ and $\pm 5/2$, we expect only one CEF excitation from the ground state according to the selection rule for allowed transitions, $\Delta J_z = \pm 1$. A similar situation will arise when pure $J_z = \pm 5/2$ is a ground state. In both these situations, we expect excited state transitions when temperature is high enough to populate the first excited state.

The crystal-field Hamiltonian for the cubic site (H_{Cubic}) and tetragonal site (H_{Tetra}) Ce atoms are given by

$$
\begin{aligned}
H_{\text{Cubic}} &= B_4^0 \left[O_4^0 + 5O_4^4 \right], \\
H_{\text{Tetra}} &= B_2^0 O_2^0 + B_4^0 O_4^0 + B_4^4 O_4^4,
\end{aligned}
\tag{1}
$$

where B_n^m are CEF parameters and O_n^m are Stevens operators. For the cubic site one can determine the value of $B_4^0 = \Delta_{\text{CEF}}/360$, where Δ_{CEF} is the crystal-field splitting energy between Γ_7 and Γ_8. However, this gives only magnitude of B_4^0, not the sign. The sign of B_4^0 (i.e., ground state Γ_7 for positive B_4^0 or Γ_8 for negative B_4^0) can be determined using the ratio of the INS peak and quasielastic linewidth. The calculated ratio of INS/EQ is 3.1935 for Γ_7 as a ground state and is 0.6157 for Γ_8 as a ground state.

In order to gain detailed information on the number of CEF excitations and the energy levels scheme, we have analyzed the Q-integrated one-dimensional (1D) energy cuts made from the low-Q region (0 to 3 Å^{-1}). The phonon background was subtracted using the scaled high-angle (110° to 135°) data for 23 and 50 meV. The scaling factor was estimated using similar measurements on the nonmagnetic reference compound LaRhSn$_3$ on MARI. Figure 4 shows the 1D energy cuts at 4.5 and 50 K from the 11-meV data. The data were
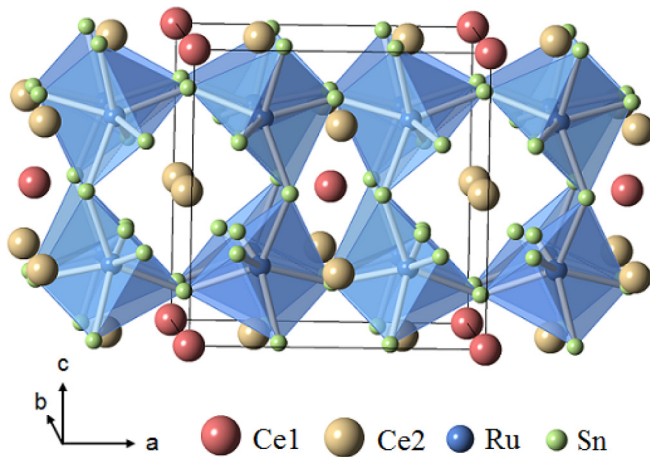

FIG. 2. LaRuSn$_3$-type cubic (space group $Pm\bar{3}n$, No. 223) crystal structure of CeRuSn$_3$. The spheres represent Ce, Ru and Sn atoms in decreasing order of sizes. Ru atoms are located within the trigonal RuSn$_6$ prisms.
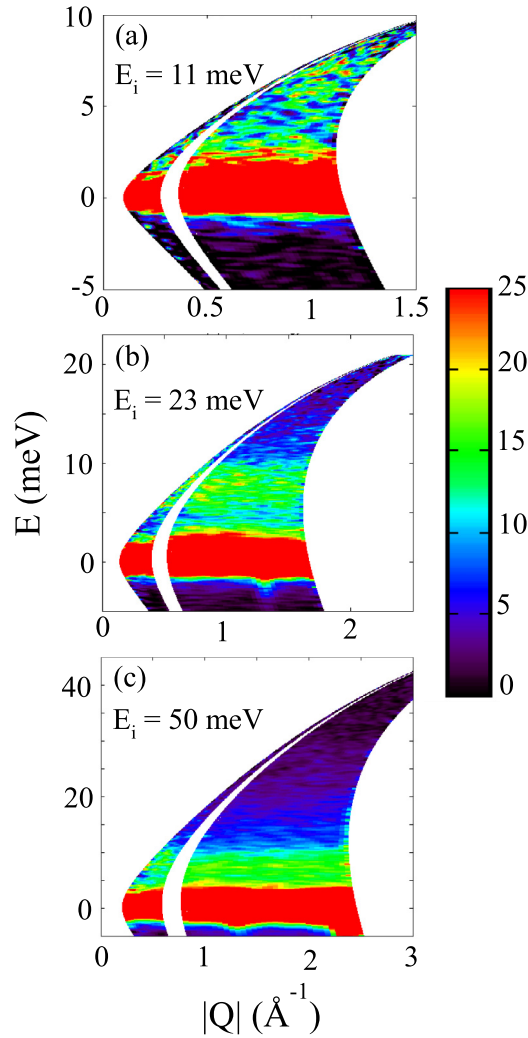
FIG. 3. Color-coded contour map of inelastic neutron scattering intensity of CeRuSn$_3$ measured at 4.5 K with incident energy (a) $E_i = 11$, (b) 23, and (c) 50 meV on the HET spectrometer plotted as a function of energy transfer E and wave-vector transfer $|Q|$.

FIG. 4. Q-integrated inelastic magnetic scattering intensity vs energy transfer of CeRuSn$_3$ at $|Q| = 0.82$ Å^{-1} measured with $E_i = 11$ meV at (a) 4.5 and (b) 50 K. The solid lines are the fits of the data and the dashed and dash-dotted lines are the different components of the fits.

analyzed using the instrument resolution function convoluted with Lorentzian line shape for both quasielastic and inelastic excitations. The population factor and magnetic form factor of Ce^{3+} ion were also included in the fitting function. It is clear that the data at both the temperatures fit very well to a QE peak plus one inelastic peak. The value of quasielastic linewidth estimated from 11 meV data at 4.5 K is $\Gamma_{QE}(4.5K) = 0.27(3)$ meV and $\Gamma_{QE}(50K) = 0.73(9)$. Taking the value of $\Gamma_{QE}(4.5K)$ at 4.5 K as $T \to 0$ K value we have estimated $T_K = 3.1(2)$ K using the relation $\Gamma_{QE} = k_B T_K$, which is in excellent agreement with that estimated from the scaling of magnetoresistance, $T_K = 3.2(1)$ K (see Sec. IV C). Further, the total susceptibility estimated from the QE (0.092 emu/mole) peak and INS (0.0007 emu/mole) peak is 0.0927 emu/mole at 4.5 K, which is also in good agreement with the measured susceptibility [19].

As there is not much coverage of Q range near 5 meV in data from $E_i = 11$ meV run, we will now discuss INS excitations from $E_i = 23$ and 50 meV. Figure 5 shows the magnetic scattering estimated from the 23 meV data at 4.5
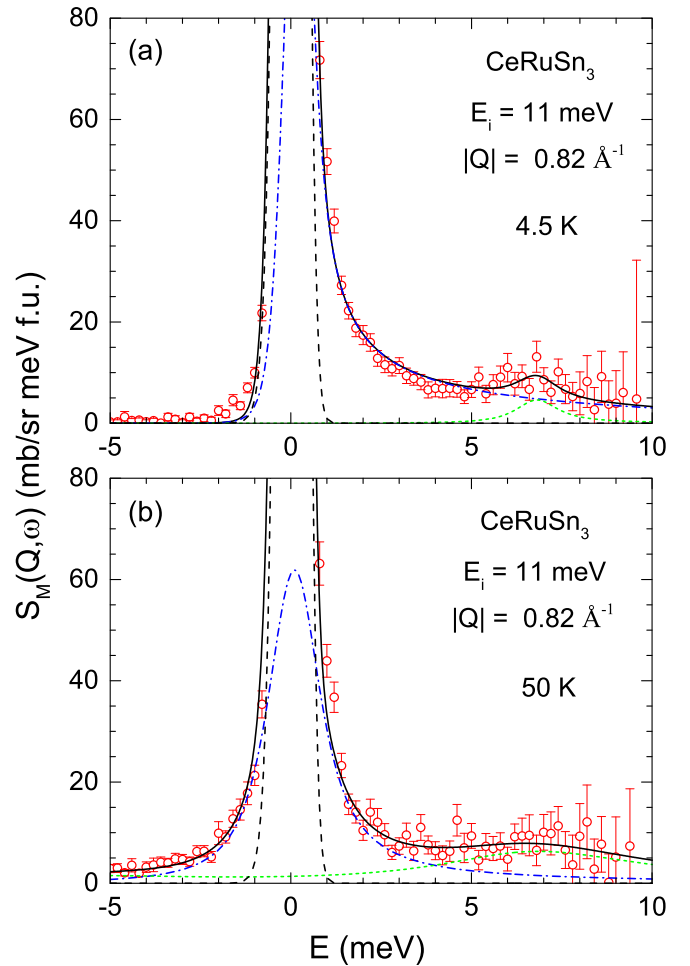
and 70 K. A clear sign of a broad magnetic excitation can be seen at 6–8 meV at 4.5 K. Here we have shown fit to one INS peak, which yields a peak position of 7.4 meV with linewidth of 1.7(2) meV. It can be seen that although the fit look reasonably good, there is a possibility to have another weak peak below 7.5 meV. We therefore also tried to fit the 4.5 K data with two possible INS peaks, and found that there are two INS excitations at 6.2 and 8.2 meV [inset of Fig. 5(a)]. The 23 meV data at 70 K in [Fig. 5(b)] could not be fitted with only one INS peak near 7.4 meV and in order to obtain a reasonable fit we had to add another peak near 13 meV. As we did not observe 13 meV peak at 4.5 K in the 23 meV data [Fig. 5(a)] or in 50 meV data (Fig. 6), we attribute this peak near 13 meV to an excited state transition from the 6.2 meV (or 8.2 meV) to possible CEF level at 19.2 (or 21.2) meV. The intensity of the transition from the ground state to 19.2 or 21.2 meV level seems to be extremely weak.

As we do not have enough information on two separate QE contributions (one from cubic site and another from tetragonal site) and also since there is not enough information on possible three INS excitations (one for cubic site and two for tetragonal
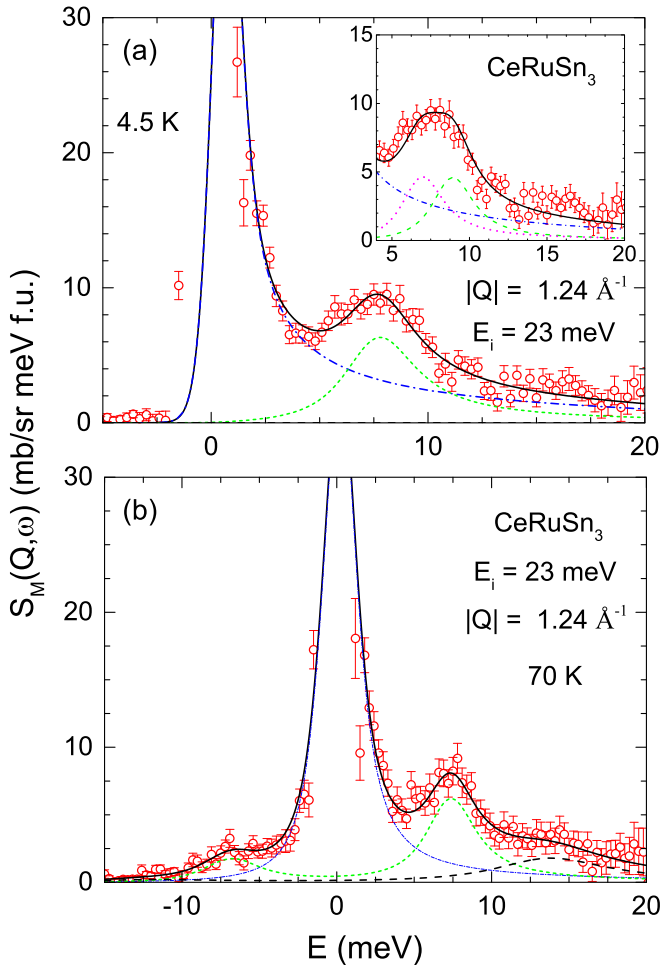
FIG. 5. Q-integrated inelastic magnetic scattering intensity vs energy transfer of CeRuSn$_3$ at $|Q| = 1.24$ Å^{-1} measured with $E_i =$ 23 meV at (a) 4.5 and (b) 70 K. The solid lines are the fits of the data and the dashed and dash-dotted lines are the different components of the fits. The inset in (a) shows the fit of 4.5 K data with two inelastic peaks.

site) from the ground state (the CEF excitations from the cubic and tetragonal sites are not resolved), it is not possible to perform a quantitative analysis of the INS data of CeRuSn$_3$ using two CEF contributions (H_{Cubic} and H_{Tetra}). We therefore use the magnetic contribution to specific heat (see below) in conjunction with the CEF energy level results from INS to determine the ground states of two Ce sites on CeRuSn$_3$. We have checked that the observed magnetic scattering intensity obey the neutron sum rules, $\int S(Q,\omega)/F^2(Q)\, d\omega = 48.6\, \mu_{\text{eff}}^2$. The analysis of 11 meV (using quasielastic intensity) data and 23 meV (using inelastic intensity) data together gave $\mu_{\text{eff}} = 2.6\, \mu_{\text{B}}$. This shows that the Ce ions on both the Ce sites are in a 3+ state.

B. Magnetic contribution to heat capacity

In order to check the validity of the CEF level scheme deduced from the analysis of INS data we compare the CEF contribution to specific heat $C_{\text{CEF}}(T)$ calculated according to the above CEF scheme with the experimentally determined magnetic contribution to specific heat $C_{\text{mag}}(T)$, which is
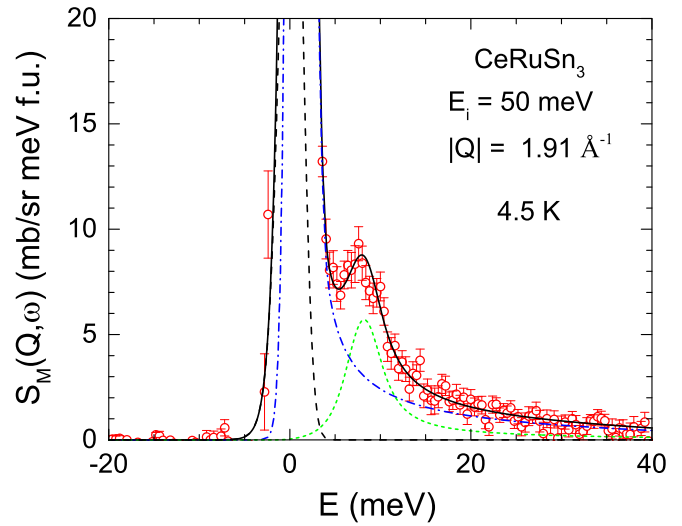

FIG. 6. Q-integrated inelastic magnetic scattering intensity vs energy transfer of CeRuSn$_3$ at $|Q| = 1.91$ Å^{-1} measured with $E_i =$ 50 meV at 4.5 K. The solid line is the fit of the data and the dashed and dash-dotted lines are the different components of the fit.

shown in Fig. 7. The $C_{\text{mag}}(T)$ was obtained by subtracting off the lattice contribution from the $C_{\text{p}}(T)$ data of CeRuSn$_3$ assuming the lattice contribution to be roughly equal to that of the nonmagnetic analog LaRuSn$_3$. The $C_{\text{mag}}(T)$ exhibits a broad Schottky-type anomaly with a maximum around 40 K, which is reproduced by the CEF model. Since there are two Ce sites (2a and 6d) with cubic and tetragonal symmetries, their contributions to specific heat according to their site multiplicities will be 25% from cubic symmetry Ce and 75% from tetragonal symmetry Ce, i.e.,

$$C_{\text{CEF}} = 0.25\, C_{\text{CEF Ce Cubic}} + 0.75\, C_{\text{CEF Ce Tetra}}, \qquad (2)$$

where $C_{\text{CEF Ce Cubic}}$ represents the contribution from cubic site Ce and $C_{\text{CEF Ce Tetra}}$ that from tetragonal site Ce.

The CEF contribution to specific heat is obtained as [26]

$$C_{\text{CEF}}(T) = \left(\frac{R}{T^2}\right)\left[\sum_i g_i e^{-\Delta_i/T} \sum_i g_i \Delta_i^2 e^{-\Delta_i/T} \right.$$
$$\left. - \left(\sum_i g_i \Delta_i e^{-\Delta_i/T}\right)^2\right]\left(\sum_i g_i e^{-\Delta_i/T}\right)^{-2}, \quad (3)$$

where g_i are the degeneracies of the CEF levels having energies Δ_i. Accordingly, for a two-level case, one obtains

$$C_{\text{CEF}}(T) = R\left(\frac{\Delta_1}{T}\right)^2 \frac{g_0 g_1 e^{-\Delta_1/T}}{(g_0 + g_1 e^{-\Delta_1/T})^2}, \qquad (4)$$

and that for the three-level case,

$$C_{\text{CEF}}(T) = \left(\frac{R}{T^2}\right)\left[g_0 g_1 \Delta_1^2 e^{-\Delta_1/T} + g_0 g_2 \Delta_2^2 e^{-\Delta_2/T}\right.$$
$$\left. + g_1 g_2 (\Delta_1 - \Delta_2)^2 e^{-(\Delta_1+\Delta_2)/T}\right]$$
$$\times (g_0 + g_1 e^{-\Delta_1/T} + g_2 e^{-\Delta_2/T})^{-2}, \qquad (5)$$

where g_0, g_1, and g_2 are the degeneracies of the ground, first excited, and second excited states, respectively, and Δ_1 and
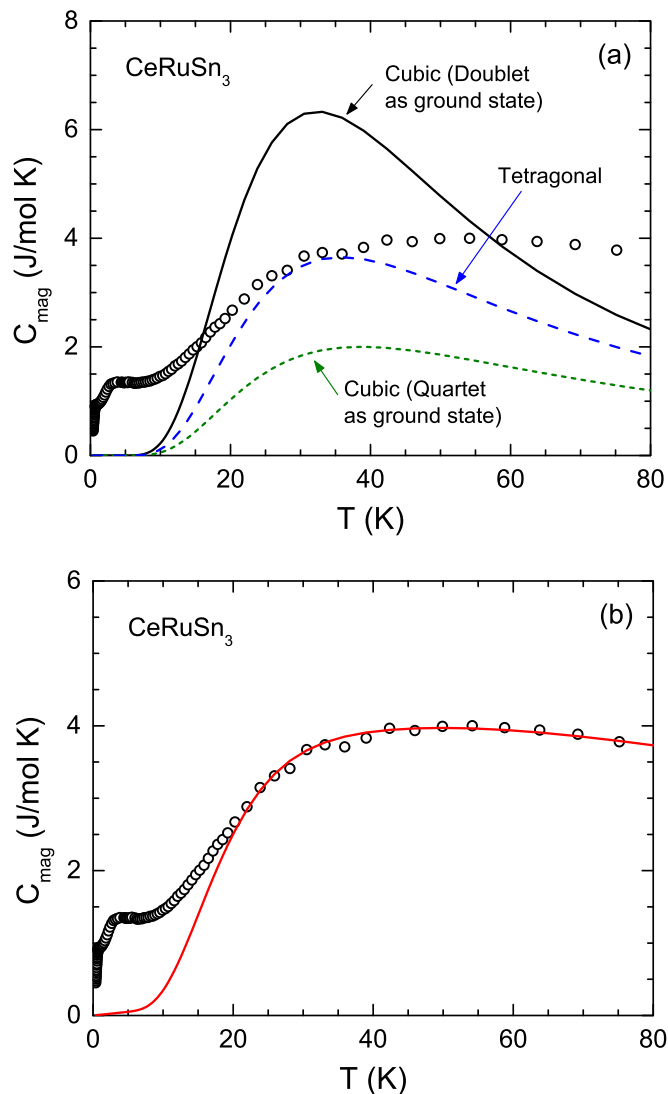
FIG. 7. Magnetic contribution to specific heat C_{mag} for CeRuSn$_3$ as a function of temperature T. The solid and dashed curves represent the crystal electric field (CEF) contributions to specific heat $C_{CEF}(T)$ for (a) two level (splitting energy 7.4 meV) CEF scheme for individual cubic and tetragonal sites, and (b) according to the sum $C_{CEF} = 0.25\, C_{CEF\,Ce\,Cubic} + 0.75\, C_{CEF\,Ce\,Tetra} + \gamma T$ taking into account for two Ce sites as discussed in text.

Δ_2 are the energies of the first and second excited states, respectively, with respect to the ground state.

As shown in Sec. IV A, the INS data (Fig. 5) could be fitted with one broad peak (7.4 meV) or two unresolved peaks (6.2 and 8.2 meV), therefore we consider both cases for estimating $C_{CEF}(T)$. First, we estimate $C_{CEF}(T)$ for two level CEF scheme (one INS peak) with an energy separation of 7.4 meV, which could be the excitation from either of cubic or tetragonal Ce sites. The $C_{CEF}(T)$ obtained [according to Eq. (4)] for both cases (cubic Ce site and tetragonal Ce site) are shown in Fig. 7(a). As discussed above, for cubic symmetry, the CEF splits the sixfold degenerate state of Ce into a doublet and a quartet, therefore for the cubic case we have considered two possibilities: (a) ground state is a doublet and (b) ground state is quartet. On the other hand, for tetragonal

symmetry the CEF splits the sixfold degenerate state of Ce into three doublets, therefore the $C_{CEF}(T)$ was calculated for two doublets separated by 7.4 meV. It is evident from Fig. 7(a) that the $C_{mag}(T)$ is not properly represented by a two-level CEF scheme (one INS peak) in either of the two cases.

Next, we estimate $C_{CEF}(T)$ for the case of two possible INS peaks at 6.2 and 8.2 meV according to Eq. (2), which takes into account for contributions from both cubic and tetragonal Ce sites. The $C_{CEF}(T)$ estimated according to Eq. (2) is shown by the solid red curve in Fig. 7(b). The $C_{CEF\,Ce\,Cubic}$ was estimated according to Eq. (4) for the quartet as ground state and doublet as excited state at 8.2 meV, i.e., $g_0 = 4$, $g_1 = 2$, and $\Delta_1 = 8.2$ meV. The $C_{CEF\,Ce\,Tetra}$ was estimated according to Eq. (5) for a ground-state doublet at 0 meV, the first excited doublet at 6.2 meV and second excited state at 19.2 meV, i.e., for $g_0 = g_1 = g_2 = 2$, $\Delta_1 = 6.2$ meV, and $\Delta_2 = 19.2$ meV. In addition to contributions from $C_{CEF\,Ce\,Cubic}$ and $C_{CEF\,Ce\,Tetra}$, a γT term corresponding to $\gamma = 10$ mJ/mol K^2 was added to account for high γ of CeRuSn$_3$ that was not properly accounted by the phonon subtraction (equivalent to the specific heat of LaRuSn$_3$, which has much lower γ than that of CeRuSn$_3$). A very reasonable agreement is found between the experimental $C_{mag}(T)$ data and the calculated $C_{CEF}(T)$ in this case, thus supporting the possibility of two unresolved peaks in INS spectra.

C. Magnetoresistance and Kondo temperature

The $\rho(H)$ data at different T [19] allow us to estimate the Kondo temperature within the Schlottmann's description of single-ion Kondo behavior of the Bethe ansatz technique to calculate the magnetoresistance in the Coqblin-Schrieffer model for impurity angular momenta $J \leqslant 5/2$ [27]. Within Schlottmann's model, for a given value of J, a universal scaling of MR is found with H and T. The scaling field $H^*(T)$ is given by [27]

$$H^*(T) = H^*(0) + \frac{k_B T}{g\mu}, \tag{6}$$

where k_B is Boltzmann's constant, g is the Landé factor, μ is the moment of Kondo ion and the Kondo field $H^*(0)$ is related to Kondo temperature T_K by

$$H^*(0) = \frac{k_B}{g\mu} T_K. \tag{7}$$

The normalized resistivity $\rho(H)/\rho(0)$ of CeRuSn$_3$ as a function of the reduced field $H(T)/H^*(T)$ is shown in Fig. 8. The solid red curve in Fig. 8 represents the Schlottmann's scaling curve for a CEF-split Kramers doublet ground state with an effective $J = 1/2$ (or $S = 1/2$) of the Ce^{3+} ion. A very reasonable agreement is observed between the theoretical curve and the H and T scaled experimental MR data. A plot of H^* versus T is shown in the inset of Fig. 8. A fit to the $H^*(T)$ by Eq. (6) shown by solid line in the inset of Fig. 8 gives the Kondo temperature $T_K = 3.2(1)$ K, in excellent agreement with $T_K = 3.1(2)$ K estimated from the neutron quasielastic linewidth above.

It should be noted though that because of the presence of two Ce sites, where for cubic symmetry site Ce ions neutron scattering and specific heat data suggest a quartet to be the ground state, one would not expect the model based on
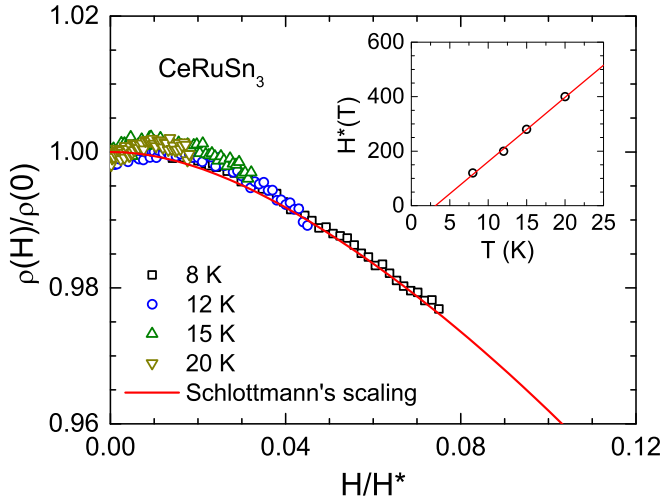
FIG. 8. Scaled magnetoresistance $\rho(H)/\rho(0)$ vs reduced field H/H^* of CeRuSn$_3$ for various temperatures. Solid curve represents Schlottmann's scaling curve for $J = 1/2$. (Inset) Scaling field H^* versus temperature T. Solid line is a linear fit of $H^*(T)$ data.

effective pseudo spin $J = 1/2$ to describe the MR data very precisely. Nevertheless, as the majority (three fourths) of Ce ions belong to tetragonal symmetry site having a doublet as ground state, the MR data are reasonably approximated by the model of Schlottmann's scaling for $J = 1/2$. Furthermore, from Fig. 8, we note that at low fields the MR data show a positive curvature, which is different from the case of CeRhSn$_3$ where no such positive curvature is observed [20], though they both have negative curvature at higher fields. This difference possibly reflects that magnetic exchange in CeRuSn$_3$ is of antiferromagnetic nature whereas CeRhSn$_3$ has a ferri-/ferro-magnetic exchange interaction.

Another estimate of T_K follows from the Weiss temperature using the relation [28] $T_K \approx |\theta_p|/4.5$, which for $\theta_p = -17.2(3)$ K of CeRuSn$_3$ [19] gives $T_K \approx 3.8$ K, which is very close to the above estimated values of T_K. A broad hump near 3 K in the $C_{mag}(T)$ data (Fig. 7) could be associated with T_K.

A rough estimate of high-T Kondo temperature T_K^h can be obtained from the value of γ within the Coqblin-Schrieffer model using the relation [29–31]

$$T_K^h = \frac{W J \pi R}{3\gamma} \qquad (8)$$

applicable to a dense Kondo system, where $W = 0.1026 \times 4\pi$ is the Wilson number, R is the molar gas constant and $J = 5/2$ for Ce^{3+}. This for $\gamma = 212(2)$ mJ/mol K^2 [19] gives $T_K^h = 132$ K. This value of T_K^h is close to the value $T_K^h = 120$ K obtained by Fukuhara *et al.* [16] using the Hamman-Fisher law. However, our value of $T_K \approx 3.2$ K is much lower than the value $T_K = 20$ K they obtained using the Hamman-Fisher law [16].

V. CeRhSn$_3$

A. Inelastic neutron scattering study

The color-coded intensity maps showing INS scattering responses from CeRhSn$_3$ and LaRhSn$_3$ measured with $E_i = 50$ meV at $T = 4.5$ K are shown in Fig. 9. While at low-Q no
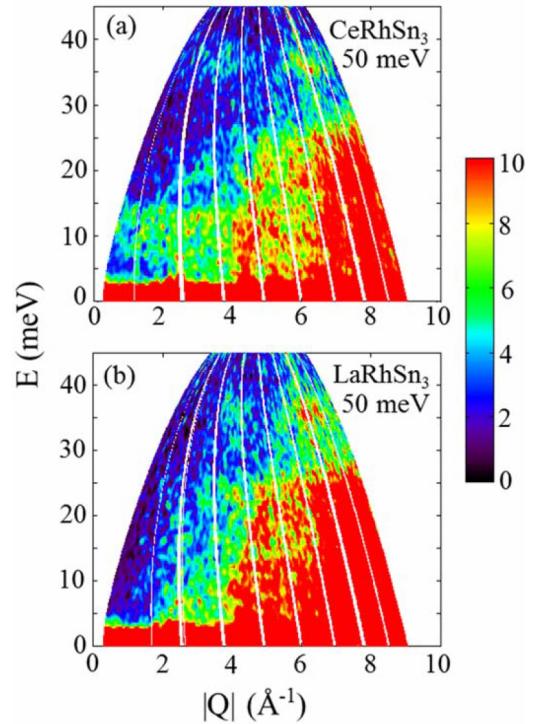

FIG. 9. Color-coded contour map of inelastic neutron scattering intensity of (a) CeRhSn$_3$ and (b) LaRhSn$_3$ measured at 4.5 K with incident energy $E_i = 50$ meV on the MARI spectrometer plotted as a function of energy transfer E and wave vector transfer $|Q|$.

excitation is seen for LaRhSn$_3$, three magnetic excitations near 7.0, 12.2, and 37.2 meV are clearly evidenced for CeRhSn$_3$. The magnetic scattering $S_M(Q,\omega)$ to CeRhSn$_3$ INS response was obtained after subtracting the phonon background using the similar INS measurement on the nonmagnetic reference compound LaRhSn$_3$. The $S_M(Q,\omega) = S(Q,\omega)_{CeRhSn_3} - \alpha S(Q,\omega)_{LaRhSn_3}$ with $\alpha = 0.75$, the ratio of neutron scattering cross sections of CeRhSn$_3$ and LaRhSn$_3$. The 1D energy cuts at 4.5 K from the 23 and 50 meV data in the low-Q region (0 to 3 Å^{-1}) are shown in Figs. 10 and 11(a) for $E_i = 23$ and 50 meV, respectively. The three magnetic excitations at 7.0, 12.2, and 37.2 meV are very clear in the 1D cuts of CeRhSn$_3$ INS data in Figs. 10 and 11(a). We attribute these excitations to the crystal-field excitations from the two Ce sites, one for the cubic Ce site (most probably near 7.0 meV) and another two from the tetragonal Ce site. As the raw data shown in Fig. 9 do not show any magnetic excitation near 19 meV, the weak peak near 19 meV in Fig. 11 seems to be a spurious artifact consequent to the phonon subtraction procedure or background scattering of unknown origin (see Appendix, Fig. 13). We also measured the INS response at 125 K for $E_i = 50$ meV [Fig. 11(b)], which did not show any additional excitation towards the transition among excited states.

As in the case of CeRuSn$_3$, the INS data were analyzed using the Lorentzian shape for both quasielastic and inelastic excitations, the fitting is shown in Fig. 10. The fit of 23 meV INS data yielded the quasielastic linewidth at 4.5 K, $\Gamma_{QE}(4.5K) = 0.4(1)$ meV. This in turn gives $T_K = 4.6 \pm 1.2$ K, which is close to but somewhat higher than the previous estimate of $T_K = 2.4$ K that was obtained from the scaling
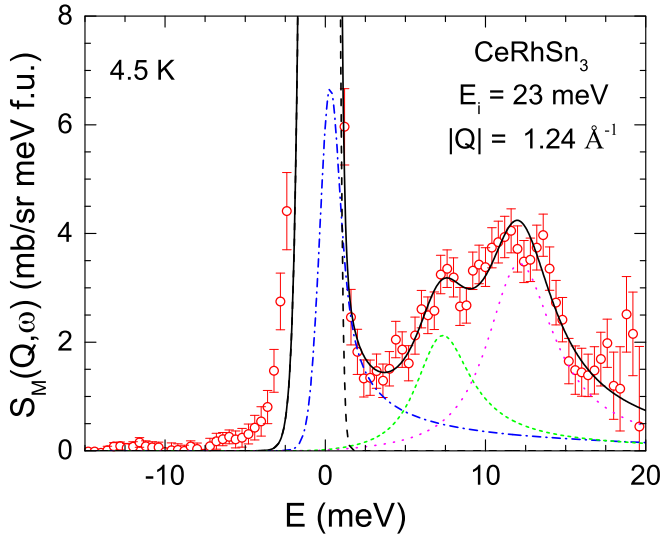
FIG. 10. *Q*-integrated inelastic magnetic scattering intensity vs energy transfer of CeRhSn$_3$ at $|Q| = 1.24$ Å^{-1} for $E_i = 23$ meV measured at 4.5 K on MARI. The solid line is the fit of the data and the dashed and dash-dotted lines are the different components of the fits.

of magnetoresistance [20]. For a precise estimate of T_K from Γ_{QE}, the INS data should have been collected at low incident energy. However, as we do not have INS data at energy lower than 23 meV, we used the Γ_{QE} from the INS data measured at 23 meV to estimate T_K, therefore this estimate of T_K may not be very accurate. The $\theta_p = -12.2$ K of CeRhSn$_3$ [20] gives $T_K \approx 2.7$ K.

Further, we analyzed the INS data of CeRhSn$_3$ using CEF contributions given in Eq. (1), which takes into account of two crystallographic sites. Our simultaneous analysis of the 50 meV INS data at 4.5 and 125 K yielded the best fit for the CEF parameters listed in Table II. The fit of the 50 meV INS data at 4.5 and 125 K are shown in Fig. 11. The analysis shows that the ground state for the cubic site is a quartet and that for the tetragonal site is a doublet, which agrees well with the ground state of CeRuSn$_3$ inferred from the combined analysis of heat capacity and INS data in Sec. IV. The CEF wave functions obtained for the cubic site Ce are

$$\Psi_1 = (0.4082)\left|\pm\tfrac{3}{2}\right\rangle + (0.9129)\left|\mp\tfrac{5}{2}\right\rangle,$$
$$\text{and } \left|\pm\tfrac{1}{2}\right\rangle, \tag{9}$$
$$\Psi_2 = (0.9129)\left|\pm\tfrac{3}{2}\right\rangle - (0.4082)\left|\mp\tfrac{5}{2}\right\rangle$$

TABLE II. Crystal-field parameters B_n^m and splitting energies Δ_i of excited states (with respect to ground state, $\Delta_0 \equiv 0$) obtained from the analysis of the inelastic neutron scattering data of CeRhSn$_3$.

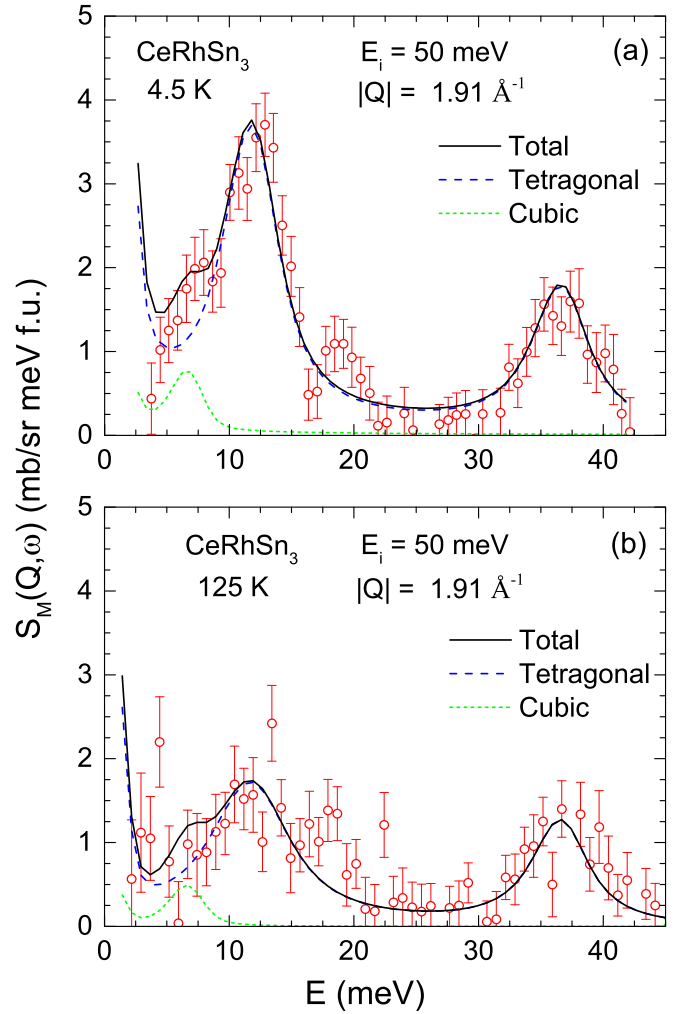|	Cubic	Tetragonal
B_2^0 (meV)		$+1.62(1)$
B_4^0 (meV)	-0.019	$+0.073(8)$
B_4^4 (meV)		$-0.042(1)$
Δ_1 (meV)	6.84	12.04
Δ_2 (meV)		36.97

FIG. 11. *Q*-integrated inelastic magnetic scattering intensity vs energy transfer of CeRhSn$_3$ at $|Q| = 1.91$ Å^{-1} measured with $E_i = 50$ meV at (a) 4.5 and (b) 125 K. The solid lines are the fits of the data by CEF model accounting for two Ce sites together with the contributions for cubic and tetragonal sites shown by dashed curves. Note: the apparent weak peak near 19 meV is an artifact due to phonon.

with quartet Ψ_1 as ground state and doublet Ψ_2 as first excited state at 6.84 meV. The CEF wave functions for the tetragonal site Ce are

$$\Psi_1 = (0.9995)\left|\pm\tfrac{3}{2}\right\rangle + (0.0302)\left|\mp\tfrac{5}{2}\right\rangle,$$
$$\Psi_2 = \left|\pm\tfrac{1}{2}\right\rangle, \tag{10}$$
$$\Psi_3 = (-0.0302)\left|\pm\tfrac{3}{2}\right\rangle + (0.9995)\left|\mp\tfrac{5}{2}\right\rangle.$$

The energy eigenvalues for the three doublets Ψ_1 (ground state), Ψ_2 (first excited state), and Ψ_3 (second excited state) are 0, 12.04 and 36.97 meV, respectively.

B. Magnetic contribution to heat capacity

The $C_{\text{mag}}(T)$ data of CeRhSn$_3$ are shown in Fig. 12 and the CEF contribution to specific heat $C_{\text{CEF}}(T)$ estimated for the above obtained CEF level scheme according to Eq. (2) is shown by the solid red curve. An additional γT [over
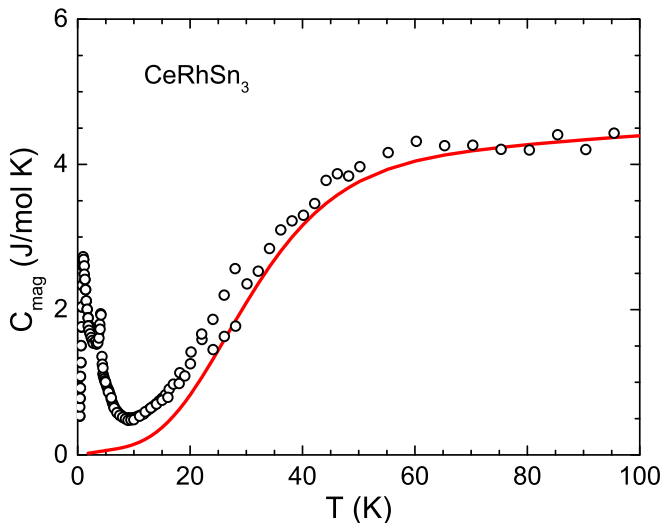
FIG. 12. Magnetic contribution to specific heat C_{mag} for CeRhSn$_3$ as a function of temperature T. The crystal electric field (CEF) contributions to specific heat according to the CEF level scheme obtained from the analysis of the inelastic neutron scattering data corresponding to the sum $C_{CEF} = 0.25\, C_{CEF\,Ce\,Cubic} + 0.75\, C_{CEF\,Ce\,Tetra} + \gamma T$.

that of LaRhSn$_3$ that was subtracted off to obtain $C_{mag}(T)$] corresponding to $\gamma = 10$ mJ/mol K^2 was added to calculated $C_{CEF}(T)$ to compare with $C_{mag}(T)$ data. A very reasonable agreement between the experimental $C_{mag}(T)$ data and the calculated $C_{CEF}(T)$ supports the obtained CEF level scheme.

VI. DISCUSSION

It is interesting to note that despite having a very similar Kondo temperature, the compounds CeRuSn$_3$ and CeRhSn$_3$ exhibit very different physical properties. While CeRuSn$_3$ does not show long-range magnetic order down to 84 mK [19] and is situated close to an antiferromagnetic QCP, CeRhSn$_3$ exhibits complex magnetic order below 4 K with dominant ferri-/ferro-magnetic interaction [20]. Apparently, in the case of CeRuSn$_3$, the Kondo interaction wins over the RKKY interaction and suppresses the long-range ordering of Ce^{3+} moments, whereas in the case of CeRhSn$_3$, RKKY interaction dominates over the Kondo interaction leading to a long-range ordering. The difference between the magnetic behaviors of CeRuSn$_3$ and CeRhSn$_3$ seems to be related to the presence of transition metals Ru ($4d^7 5s^1$) and Rh ($4d^8 5s^1$), having different number of $4d$ electrons. The extra d electron in Rh moves CeRhSn$_3$ towards more localized nature than CeRuSn$_3$. Such effect of electron doping and shift towards more localized limit has also been observed in Ce(Ru$_{1-x}$Rh$_x$)$_2$Al$_{10}$ [32,33] and Ce(Fe$_{1-x}$Rh$_x$)$_2$Al$_{10}$ [34].

The strength of hybridization between the conduction electron and the $4f$ electron (c-f hybridization) is transition metal dependent. The Kondo temperature depends on c-f hybridization strength Γ and density of states at Fermi level $\mathcal{D}(E_F)$, $T_K \sim \exp(-|\epsilon_f|/\Gamma^2 \mathcal{D}(E_F))$ where ϵ_f is the binding energy of the $4f$ level. The γ values of about 100 mJ/mol K^2 for CeRhSn$_3$ [20] and 212 mJ/mol K^2 for CeRuSn$_3$ [19] clearly reflect that CeRuSn$_3$ has much larger $\mathcal{D}(E_F)$ than that

of CeRhSn$_3$. The similar values of T_K despite the different $\mathcal{D}(E_F)$ can thus be naively considered to be an indication for the two compounds to have different c-f hybridization strength. Their different inelastic neutron scattering responses and hence crystal-field excitations possibly reflect the difference in hybridization strength associated with different numbers of $4d$ electrons.

The ternary compounds CeRhSi$_3$ and CeRuSi$_3$ both having BaNiSn$_3$-type noncentrosymmetric tetragonal (space group $I4\,mm$) structure also show different physical properties because of the different degree of c-f hybridization by transition metals Rh and Ru. CeRhSi$_3$ is found to order antiferromagnetically below 1.6 K and exhibit pressure induced superconductivity at a critical pressure of about 1.2 GPa [35,36]. In contrast, with a dominant Kondo interaction CeRuSi$_3$ remains paramagnetic [37]. The INS study revealed evidence for hybridization gap in CeRuSi$_3$ [38]. A similar magnetically ordered versus paramagnetic ground state for Rh and Ru has been observed in the case of ThCr$_2$Si$_2$-type tetragonal (space group $I4/mmm$) structure compounds CeRh$_2$Si$_2$ and CeRu$_2$Si$_2$. While CeRh$_2$Si$_2$ orders antiferromagnetically below 36 K [39,40], no evidence of long-range ordering is seen down to 170 μK in CeRu$_2$Si$_2$ [41]. An extremely small static electronic moment of the order of $10^{-3}\mu_B$ was reported from μSR measurement on CeRu$_2$Si$_2$ [42]. The INS study shows different CEF splitting energies in these compounds: 0, 32, and 33 meV for CeRu$_2$Si$_2$ and 0, 30, and 52 meV for CeRh$_2$Si$_2$ [43]. A recent angle-resolved photoelectron emission study on CeRh$_2$Si$_2$ suggests a significant mixing of Ce $4f^1$ and $4f^0$ states even in the antiferromagnetic state demonstrating the importance of hybridization effects [44].

VII. CONCLUSIONS

We have performed inelastic neutron scattering experiments on two Kondo lattice heavy fermion systems CeRuSn$_3$ and CeRhSn$_3$. An estimate of Kondo temperature is made from the neutron quasielastic linewidth, which gave a value of $T_K = 3.1(2)$ K for CeRuSn$_3$ in excellent agreement with the estimate of $T_K = 3.2(1)$ K from the scaling of magnetoresistance data. A trivalent state of Ce ions for both the cubic and tetragonal Ce sites is inferred from the neutron intensity sum rule. In contrast to the expected three CEF excitations (one from cubic and two from tetragonal Ce cites), the INS data of CeRuSn$_3$ reveal a broad excitation near 6–8 meV. The analysis of INS data using a CEF model shows the possibility of two unresolved CEF excitations near 6.2 and 8.2 meV with an overall CEF splitting of about 19.2 meV, which is supported by the analysis of $C_{mag}(T)$ data based on the CEF model. The INS data of CeRhSn$_3$ on the other hand clearly exhibit three CEF excitations near 7.0, 12.2, and 37.2 meV. From the neutron quasielastic linewidth analysis the T_K for CeRhSn$_3$ is estimated to be $T_K \approx 4.6$ K. The ground state of Ce^{3+} in both the compounds is found to be quartet for the Ce^{3+} ions occupying the cubic site and doublet for the Ce^{3+} ions occupying the tetragonal site. The crystal-field parameters and ground-state wave functions for both the cubic and tetragonal sites of Ce^{3+} were determined for CeRhSn$_3$.

It appears that the transition metal (Rh and Ru with different number of $4d$ electrons) plays a decisive role in controlling the

c-f hybridization strength which in turn governs the physical properties, manifesting different crystal-field excitations and hence different inelastic neutron scattering responses for the two compounds. Further investigations of hybridization strength would be enlightening for the understanding of the role of hybridization in determining the nature of electronic ground state of these compounds.

ACKNOWLEDGMENTS

APPENDIX: COMPARISON OF SCATTERING FROM CeRhSn$_3$ AND LaRhSn$_3$

A comparison of the Q-integrated INS scattering from CeRhSn$_3$ and LaRhSn$_3$ at 4.5 K at low Q (1.91 Å^{-1}) and high Q (7.31 Å^{-1}) is shown in Fig. 13 for $E_i = 50$ meV. In order to estimate the phonon contribution to INS data of CeRhSn$_3$ the INS data of LaRhSn$_3$ have been scaled by a factor $\alpha = 0.75$ equivalent to the ratio of neutron scattering cross sections of CeRhSn$_3$ and LaRhSn$_3$. The difference plot $S_M(Q,\omega) = S(Q,\omega)_{\mathrm{CeRhSn_3}} - \alpha S(Q,\omega)_{\mathrm{LaRhSn_3}}$ is presented in Fig. 11(a) showing the magnetic scattering from CeRhSn$_3$ at low Q. A comparison of low-Q and high-Q $S(Q,\omega)$ of CeRhSn$_3$ shows that the weak peak near 19 meV marked with arrow, that is present even at high-Q, is not of magnetic origin. The intensity of excitations of magnetic origin decreases with increasing Q and becomes negligibly small at high enough Q. In contrast, we see that the 19 meV peak is present at both low and high Q. On the other hand, the three magnetic excitations near 7.0, 12.2, and 37.2 meV disappear at high Q. This suggests that the 19-meV peak does not originate from CEF excitations, could be due to phonon or some unknown
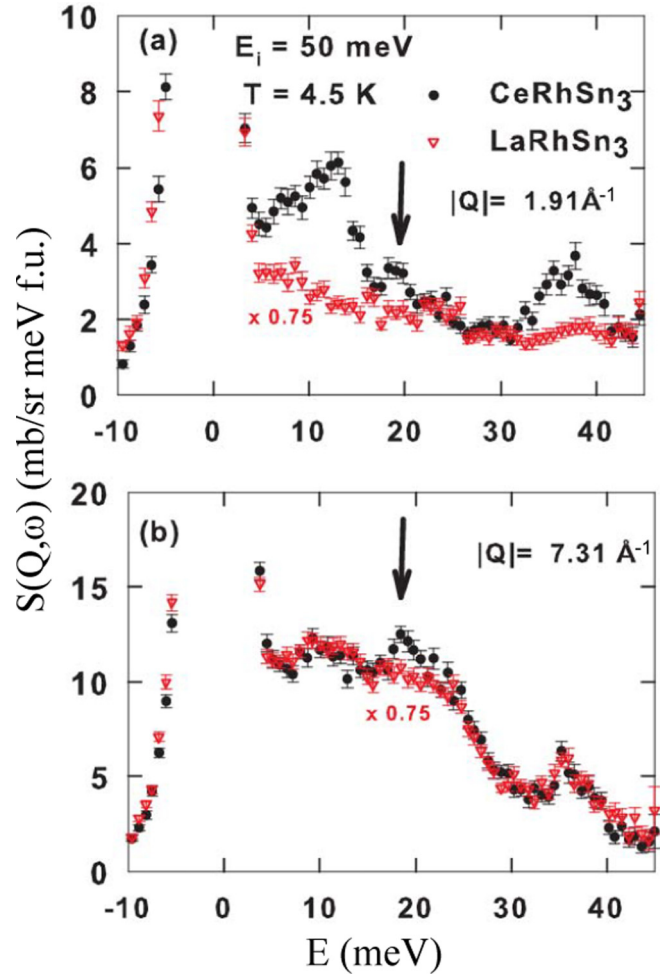

FIG. 13. Q-integrated inelastic scattering intensity versus energy transfer of CeRhSn$_3$ and LaRhSn$_3$ at (a) low $|Q| = 1.91$ Å^{-1} and (b) high $|Q| = 7.31$ Å^{-1} for $E_i = 50$ meV measured at 4.5 K on MARI. The LaRhSn$_3$ data have been scaled by a factor $\alpha = 0.75$. The arrows show the spurious peak of nonmagnetic origin near 19 meV.

background scattering. Thus the apparent weak peak near 19 meV in $S_M(Q,\omega)$ in Fig. 11 is not due to CEF excitation.

[1] G. R. Stewart, Rev. Mod. Phys. **56**, 755 (1984); **73**, 797 (2001).

[2] A. Amato, Rev. Mod. Phys. **69**, 1119 (1997).

[3] P. S. Riseborough, Adv. Phys. **49**, 257 (2000).

[4] H. v. Löhneysen, A. Rosch, M. Vojta, and P. Woelfle, Rev. Mod. Phys. **79**, 1015 (2007).

[5] C. Pfleiderer, Rev. Mod. Phys. **81**, 1551 (2009).

[6] Q. Si and F. Steglich, Science **329**, 1161 (2010).

[7] A. Thamizhavel, T. Takeuchi, T. D. Matsuda, Y. Haga, K. Sugiyama, R. Settai, and Y. Ōnuki, J. Phys. Soc. Jpn. **74**, 1858 (2005).

[8] M. Smidman, D. T. Adroja, A. D. Hillier, L. C. Chapon, J. W. Taylor, V. K. Anand, R. P. Singh, M. R. Lees, E. A.

Goremychkin, M. M. Koza, V. V. Krishnamurthy, D. M. Paul, and G. Balakrishnan, Phys. Rev. B **88**, 134416 (2013).

[9] R. Settai, I. Sugitani, Y. Okuda, A. Thamizhavel, M. Nakashima, Y. Ōnuki, and H. Harima, J. Magn. Magn. Mater. **310**, 844 (2007).

[10] D. Eom, M. Ishikawa, J. Kitagawa, and N. Takeda, J. Phys. Soc. Jpn. **67**, 2495 (1998).

[11] M. A. Continentino, S. N. de Medeiros, M. T. D. Orlando, M. B. Fontes, and E. M. Baggio-Saitovitch, Phys. Rev. B **64**, 012404 (2001).

[12] V. V. Krishnamurthy, K. Nagamine, I. Watanabe, K. Nishiyama, S. Ohira, M. Ishikawa, D. H. Eom, T. Ishikawa, and T. M. Briere, Phys. Rev. Lett. **88**, 046402 (2002).

[13] B. Eisenmann and H. Schäfer, J. Less-Common Metals **123**, 89 (1986).

[14] T. Fukuhara, I. Sakamoto, H. Sato, S. Takayanagi, and N. Wada, J. Phys.: Condens. Matter **1**, 7487 (1989).

[15] S. Takayanagi, T. Fukuhara, H. Sato, N. Wada, and Y. Yamada, Physica B **165-166**, 447 (1990).

[16] T. Fukuhara, I. Sakamoto, and H. Sato, J. Phys.: Condens. Matter **3**, 8917 (1991).

[17] S. Takayanagi, T. Fukuhara, H. Sato, and N. Wada, Physica C **185-189**, 2643 (1991).

[18] H. Ishii, T. Hanyu, T. Fukuhara, I. Sakamoto, H. Sato, and S. Yamaguchi, J. Phys. Soc. Jpn. **62**, 811 (1993).

[19] V. K. Anand, D. T. Adroja, A. Bhattacharyya, A. D. Hillier, D. Britz, A. M. Strydom, J. W. Taylor, A. Fraile, and W. Kockelmann, J. Phys.: Conf. Ser. **592**, 012008 (2015).

[20] V. K. Anand, D. T. Adroja, A. D. Hillier, W. Kockelmann, A. Fraile, and A. M. Strydom, J. Phys.: Condens. Matter **23**, 276001 (2011).

[21] V. K. Anand, D. T. Adroja, and A. D. Hillier, Phys. Rev. B **85**, 014418 (2012).

[22] E. A. Goremychkin, R. Osborn, B. D. Rainford, R. T. Macaluso, D. T. Adroja, and M. Koza, Nature Phys. **4**, 766 (2008).

[23] V. K. Anand, D. T. Adroja, A. D. Hillier, J. Taylor, and G. Andŕe, Phys. Rev. B **84**, 064440 (2011).

[24] A. C. Larson and R. B. Von Dreele, Tech. Rep. LAUR 86-748, Los Alamos National Laboratory, 2004; B. H. Toby, J. Appl. Cryst. **34**, 210 (2001).

[25] T. Harmening, W. Hermes, M. Eul, and R. Pöttgen, Solid State Sci. **12**, 284 (2010).

[26] E. S. R. Gopal, *Specific Heats at Low Temperatures* (Plenum, New York, 1966).

[27] P. Schlottmann, Z. Phys. B **51**, 223 (1983).

[28] G. Grüner and A. Zawadowski, Rep. Prog. Phys. **37**, 1497 (1974).

[29] H. Yamamoto, M. Ishikawa, K. Hasegawa, and J. Sakurai, Phys. Rev. B **52**, 10136 (1995).

[30] V. T. Rajan, Phys. Rev. Lett. **51**, 308 (1983).

[31] A. M. Tsvelick and P. B. Wiegmann, J. Phys. C **15**, 1707 (1982).

[32] R. Kobayashi, Y. Ogane, D. Hirai, T. Nishioka, M. Matsumura, Y. Kawamura, K. Matsubayashi, Y. Uwatoko, H. Tanida, and M. Sera, J. Phys. Soc. Jpn. **82**, 093702 (2013).

[33] S.-i. Kimura, H. Tanida, M. Sera, Y. Muro, T. Takabatake, T. Nishioka, M. Matsumura, and R. Kobayashi, Phys. Rev. B **91**, 241120(R) (2015).

[34] H. Tanida, M. Nakamura, M. Sera, T. Nishioka, and M. Matsumura, Phys. Rev. B **92**, 235154 (2015).

[35] Y. Muro, D. Eom, N. Takeda, and M. Ishikawa, J. Phys. Soc. Jpn. **67**, 3601 (1998).

[36] N. Kimura, K. Ito, K. Saitoh, Y. Umeda, H. Aoki, and T. Terashima, Phys. Rev. Lett. **95**, 247004 (2005).

[37] T. Kawai, H. Muranaka, M.-A. Measson, T. Shimoda, Y. Doi, T. D. Matsuda, Y. Haga, G. Knebel, G. Lapertot, D. Aoki, J. Flouquet, T. Takeuchi, R. Settai, and Y. Ōnuki, J. Phys. Soc. Jpn. **77**, 064716 (2008).

[38] M. Smidman, D. T. Adroja, E. A. Goremychkin, M. R. Lees, D. M. Paul, and G. Balakrishnan, Phys. Rev. B **91**, 064419 (2015)

[39] T. Graf, M. F. Hundley, R. Modler, R. Movshovich, J. D. Thompson, D. Mandrus, R. A. Fisher, and N. E. Phillips, Phys. Rev. B **57**, 7442 (1998).

[40] S. Kawarazaki, M. Sato, Y. Miyako, N. Chigusa, K. Watanabe, N. Metoki, Y. Koike, and M. Nishi, Phys. Rev. B **61**, 4167 (2000).

[41] D. Takahashi, S. Abe, H. Mizuno, D. A. Tayurskii, K. Matsumoto, H. Suzuki, and Y. Ōnuki, Phys. Rev. B **67**, 180407(R) (2003).

[42] A. Amato, R. Feyerherm, F. N. Gygax, A. Schenck, J. Flouquet, and P. Lejay, Phys. Rev. B **50**, 619(R) (1994).

[43] T. Willers, D. T. Adroja, B. D. Rainford, Z. Hu, N. Hollmann, P. O. Körner, Y.-Y. Chin, D. Schmitz, H. H. Hsieh, H.-J. Lin, C. T. Chen, E. D. Bauer, J. L. Sarrao, K. J. McClellan, D. Byler, C. Geibel, F. Steglich, H. Aoki, P. Lejay, A. Tanaka, L. H. Tjeng, and A. Severing, Phys. Rev. B **85**, 035117 (2012).

[44] S. Patil, A. Generalov, M. Güttler, P. Kushwaha, A. Chikina, K. Kummer, T. C. Rödel, A. F. Santander-Syro, N. Caroca-Canales, C. Geibel, S. Danzenbächer, Y. Kucherenko, C. Laubschat, J. W. Allen, and D. V. Vyalikh, Nat. Commun. **7**, 11029 (2016).